Adiabatic quantum pumping of chiral Majorana fermions

M. Alos-Palop,[1] Rakesh P. Tiwari,[2] and M. Blaauboer[1]

[1]*Delft University of Technology, Kavli Institute of Nanoscience, Department of Quantum Nanoscience, Lorentzweg 1, 2628 CJ Delft, The Netherlands*

[2]*Department of Physics, University of Basel, Klingelbergstrasse 82, CH-4056 Basel, Switzerland*

(Received 10 May 2013; revised manuscript received 27 August 2013; published 21 January 2014)

We investigate adiabatic quantum pumping of chiral Majorana states in a system composed of two Mach-Zehnder type interferometers coupled via a quantum point contact. The pumped current is generated by periodic modulation of the phases accumulated by traveling around each interferometer. Using scattering matrix formalism we show that the pumped current reveals a definite signature of the chiral nature of the Majorana states involved in transport in this geometry. Furthermore, by tuning the coupling between the two interferometers the pump can operate in a regime where finite pumped current and zero conductance are expected.

DOI: 10.1103/PhysRevB.89.045307 PACS number(s): 73.23.−b, 73.25.+i, 74.45.+c

Introduction. Recently, a great amount of attention has been paid to the possibility of realizing Majorana quasiparticles in condensed matter systems.[1–4] Majorana-like excitations have been predicted to exist in the $\nu = 5/2$ quantum Hall state,[5,6] p-wave superconductors,[7] and semiconductor-superconductor interfaces[8–10] and on the surface of topological insulators.[11–14] Experimental progress on the latter is described in Refs. 15–19. Zero-bias conductance anomalies[20–23] associated with localized Majorana excitations have been measured recently in semiconductor-nanowire-superconductor hybrid structures.[24–28] Measurements of unconventional Josephson effects associated with these excitations have also been reported.[29,30] In addition, unique signatures of *chiral* Majorana fermions have been predicted in Mach-Zehnder[31,32] and Hanbury Brown–Twiss[33] type interferometers through conductance and noise measurements. In this article, we propose and analyze an adiabatic Majorana quantum pump which can provide conclusive evidence of the chiral nature of the Majorana modes. These *chiral* Majorana modes exist as gapless, charge-neutral edge excitations in 2D chiral p-wave superconductors (or systems equivalent to such superconductors) and should not be confused with Majorana bound states existing in 1D chiral p-wave superconductors (or systems equivalent to such superconductors).

Adiabatic pumping is a transport mechanism in meso- and nanoscale devices by which a finite dc current is generated in the absence of an applied bias by low-frequency periodic modulations of at least two system parameters (typically gate voltages or magnetic fields).[34,35] In order for electrical transport to be adiabatic, the period of the oscillatory driving signals has to be much longer than the dwell time $\tau_{\rm dwell}$ of the electrons in the system, $T = 2\pi\omega^{-1} \gg \tau_{\rm dwell}$. Adiabatic *quantum* pumping[36] refers to pumping in open systems in which quantum-mechanical interference of electron waves occurs. Recently, adiabatic topological pumping in a spin-orbit coupled semiconductor nanowire in proximity to an s-wave superconductor and subjected to a Zeeman field was studied.[37] In this study we consider an adiabatic quantum pump where the carriers responsible for transport are *chiral* Majorana fermions. A schematic of the proposed device is shown in Fig. 1. The pump consists of two superconducting islands supporting chiral Majorana edge states coupled via a quantum point contact. While the conductance in this system can be used to signal whether an unpaired Majorana bound state exists in the superconducting region or not (as was predicted in Refs. 31 and 32), it does not contain information about the chiral nature of the carriers. We show that, in contrast, the pumped current in this system exhibits definite and measurable signatures of the chiral nature of quantum transport. Furthermore, charge neutrality of the Majorana modes (limiting interactions with the environment) and the adiabatic operation of the pump makes this system attractive for studying quantum interference effects with Majorana modes in the presence of, in principle, negligible dephasing.

Majorana quantum pump. The superconducting and magnetic correlations on the surface of a topological insulator (as shown in Fig. 1, with $\hat{z}$ being the unit vector in the out-of-plane direction), as well as the gapless states at the interfaces between them, can be described by the Dirac–Bogoliubov–de Gennes (DBdG) Hamiltonian $H = \Psi^\dagger \mathcal{H} \Psi/2$. In the Nambu basis where $\Psi = (u_\uparrow, u_\downarrow, v_\downarrow, -v_\uparrow)^T$,[31] the Hamiltonian $\mathcal{H}$ is given by

$$\mathcal{H} = -i\hbar v_F \tau_z \otimes \hat{z}\cdot\vec{\sigma}\times\nabla - \mu\tau_z\otimes\sigma_0 + (\Delta\tau_+\otimes\sigma_0 + \Delta^*\tau_-\otimes\sigma_0) + M\tau_0\otimes\sigma_z. \quad (1)$$

Here $\vec{\sigma}$ and $\vec{\tau}$ represent vectors of Pauli matrices in spin space and particle-hole Nambu space, respectively. Similarly, σ_0 and τ_0 represent 2×2 identity matrices in spin and Nambu space, and $\tau^\pm = (\tau_x \pm i\tau_y)/2$. The first two terms in $\mathcal{H}$ describe the free surface states of the three-dimensional topological insulator with v_F the Fermi velocity and μ the chemical potential. We choose the coordinate system such that this surface is parallel to the x-y plane. The first term in the second line in $\mathcal{H}$ describes the superconducting proximity effect due to an s-wave superconductor. The magnetizations $M_\uparrow = (0,0,M)$ and $M_\downarrow = (0,0,-M)$ of the two ferromagnetic insulators (as shown in Fig. 1) describe the effect of Zeeman splitting as expressed by the last term in Eq. (1). Δ and M are assumed to be spatially uniform. The excitation spectrum is gapped in both the superconducting and the magnetic regions. In the superconducting region the excitation spectrum is $E_{\mathbf{k}}^{\mathcal{S}} = \sqrt{(\pm v_F|\mathbf{k}| - \mu)^2 + |\Delta|^2}$. In the magnetic region it is $E_{\mathbf{k}}^{\mathcal{M}} = \sqrt{v_F^2|\mathbf{k}|^2 + M^2} \pm \mu$ (which is gapped if $M > \mu$). Solutions of Eq. (1) also include the subgap chiral Majorana branch localized near the superconductor-ferromagnet interface with

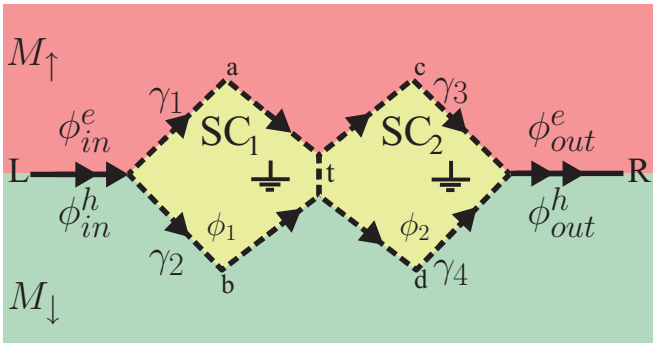

FIG. 1. (Color online) Schematic of the Mach-Zehnder interferometer studied in this paper. Two superconducting islands, SC_1 and SC_2, are connected via a point contact (t). In the left (in) and right (out) lead, two chiral Dirac fermion modes, ϕ^e and ϕ^h, propagate. The entire setup is placed on top of a 3D topological insulator. Majorana fermions γ_l ($l = 1$–4) are the mediating states in the central interferometer region. See the text for more details.

group velocity $v_m = v_F\sqrt{1-\mu^2/M^2}/(1+\mu^2/|\Delta|^2)$.[31] The amplitudes of these chiral Majorana modes are denoted by γ_l, $l \in \{1,4\}$ in Fig. 1. The interface between regions with opposite signs of magnetizations supports two chiral Dirac fermion modes. One is the electron mode with amplitude ϕ^e and the other the hole mode with amplitude ϕ^h. Within the Landauer-Büttiker scattering matrix formalism we can relate the two incoming modes $\phi^e_{\rm in}$ and $\phi^h_{\rm in}$ with two outgoing modes γ_1 and γ_2 at the left tri-junction using $(\gamma_1,\gamma_2)^T = S(E)(\phi^e_{\rm in},\phi^h_{\rm in})^T$. Particle-hole symmetry $[S(E) = S^*(-E)\tau_x]$ along with unitarity $[(S^\dagger)^{-1} = S]$ allows us to choose at $E = 0$

$$S = \frac{1}{\sqrt{2}}\begin{pmatrix} 1 & 1 \\ i & -i \end{pmatrix}. \tag{2}$$

Similarly we can relate the chiral Majorana modes γ_3 and γ_4 to outgoing electron and hole modes at the right tri-junction. In the following it is assumed that $S(E)$ is well described by its zero energy limit, which is appropriate for small energies $E \ll (v_m/v_F)\min(|\Delta|, M)$ and junctions with mirror symmetry.[31]

The Majorana modes γ_1 and γ_2 are coupled to Majorana modes γ_3 and γ_4 via the Josephson junction between the two superconductors (denoted as SC_1 and SC_2 in Fig. 1). The junction acts as a quantum point contact (QPC) for the Majorana modes and can be characterized by a 2×2 scattering matrix, $(\gamma_3,\gamma_4)^T = S_{\rm QPC}(\gamma_1,\gamma_2)^T$,[31] where

$$S_{\rm QPC} = \begin{pmatrix} r_1 & t_2 \\ t_1 & r_2 \end{pmatrix}. \tag{3}$$

Here $|t_1|^2 = 1-|r_1|^2$ and $|t_2|^2 = 1-|r_2|^2$. The properties of this QPC can be tuned by changing the phase difference $\phi_1 - \phi_2$ of the Josephson junction (as shown in Fig. 1) or by altering its shape. As explained in Ref. 31, this Josephson junction describes superconductors weakly coupled by single-electron tunneling at a point. Particle-hole symmetry and unitarity imply that r_j and t_j are real coefficients. Below we assume a symmetric Josephson junction and set $r_1 = r_2 = r$ and $t_1 = -t_2 = t$. The incoming electrons and holes can be related to the outgoing electrons and holes by the full scattering matrix of the system $(\phi^e_{\rm out},\phi^h_{\rm out})^T = S_{\rm RL}(\phi^e_{\rm in},\phi^h_{\rm in})^T$. The scattering matrix $S_{\rm RL}$ can be decomposed into $S_{\rm RL} = S^\dagger S_2 S_{\rm QPC} S_1 S$, where

$$S_1 = \begin{pmatrix} e^{i\beta_a} & 0 \\ 0 & e^{i\beta_b} \end{pmatrix},\quad S_2 = \begin{pmatrix} e^{i\beta_c} & 0 \\ 0 & e^{i\beta_d} \end{pmatrix} \tag{4}$$

denote the contribution from the phase shifts β_k ($k \in \{a,b,c,d\}$) picked up by the Majorana modes by traversing the kth arm of the interferometer. The relative phase shifts $\beta_a - \beta_b \equiv \tilde\theta_1 = \pi n_{\nu_1} + \pi + E\delta\tau_1/\hbar$ includes a contribution of π for every vortex enclosed, a Berry phase of π for spin-1/2 particles, and the dynamical phase. Similarly, $\beta_c - \beta_d \equiv \tilde\theta_2 = \pi n_{\nu_2} + \pi + E\delta\tau_2/\hbar$. Here n_{ν_1} and n_{ν_2} denote the number of vortices in SC_1 and SC_2, $\delta\tau_1 = L_a/(v_m)_a - L_b/(v_m)_b$, and $\delta\tau_2 = L_c/(v_m)_c - L_d/(v_m)_d$, where L_k and $(v_m)_k$ are the length and the velocity of the chiral Majorana mode in the kth arm of the interferometer. We then obtain

$$S_{\rm RL} = e^{i(\beta_b+\beta_d)}\begin{bmatrix} \eta_1^+ r - i\eta_2^+ t & -\eta_1^- r - i\eta_2^- t \\ -\eta_1^- r + i\eta_2^- t & \eta_1^+ r + i\eta_2^+ t \end{bmatrix}, \tag{5}$$

where $\eta_1^\pm = (1 \pm e^{i(\tilde\theta_1+\tilde\theta_2)})/2$, $\eta_2^\pm = (e^{i\tilde\theta_1} \pm e^{i\tilde\theta_2})/2$, and the (2,1) element of $S_{\rm RL}$ indicates conversion of an incoming electron in the left lead to an outgoing hole in the right lead.

Adiabatic quantum pumping. In our device the adiabatically pumped current through the Mach-Zehnder interferometer is driven by periodic modulation of the phases $\tilde\theta_1$ and $\tilde\theta_2$ as $\tilde\theta_1(t) = \theta_1 + \delta\theta_1\cos(\omega t)$ and $\tilde\theta_2(t) = \theta_2 + \delta\theta_2\cos(\omega t + \alpha)$. The total pumped current I into the right lead (see Fig. 1) can then be expressed as an integral over the area A that is enclosed in $(\tilde\theta_1, \tilde\theta_2)$ parameter space during one period, and is given by the scattering matrix expression[38,39]

$$I_{p,R} = \frac{\omega e}{2\pi^2}\int_A d\theta_1\, d\theta_2 \sum_{\substack{m\in L\\ n\in R}} {\rm Im}\{\Pi_{nm}(\theta_1,\theta_2)\} \tag{6a}$$

$$\approx \frac{\omega e}{2\pi}\,\delta\theta_1\,\delta\theta_2\,\sin\alpha \sum_{\substack{m\in L\\ n\in R}} {\rm Im}\{\Pi_{nm}(\theta_1,\theta_2)\}. \tag{6b}$$

Here

$$\Pi_{nm}(\theta_1,\theta_2) = \left(\frac{\partial S^{he}_{\rm RL}}{\partial\theta_1}\frac{\partial S^{he*}_{\rm RL}}{\partial\theta_2} - \frac{\partial S^{ee}_{\rm RL}}{\partial\theta_1}\frac{\partial S^{ee*}_{\rm RL}}{\partial\theta_2}\right)_{nm}. \tag{7}$$

Equation (6b) is valid in the bilinear response regime where $\delta\theta_1 \ll \theta_1$ and $\delta\theta_2 \ll \theta_2$ and the integral in Eq. (6a) becomes independent of the pumping contour. $S_{{\rm RL},nm}$ describes the scattering of a Dirac fermion in mode m in the left (L) lead to a Dirac fermion in mode n in the right (R) lead. The explicit adiabatic condition for this system is given by $\hbar\omega \ll \{\Delta, M, \hbar(v_m)_k/L_k\}$ ($k \in \{a,b,c,d\}$).

After calculating the derivatives of the scattering matrix coefficients using Eq. (5) and taking the imaginary part of the product, we obtain for the pumped current into the right lead of the single-mode pump of Fig. 1

$$I_{p,R} = I_0\left(rt - 2rt\sin^2\left(\frac{\theta_2}{2}\right) - t^2\sin(\theta_1-\theta_2)\right), \tag{8}$$

where $I_0 = (\omega e)/(4\pi)\,\delta\theta_1\,\delta\theta_2\,\sin\alpha$. From Eq. (8) we see that the electron (hole) charge collected in the right lead is always

mediated by the interference of two chiral Majorana modes (see also Ref. 40). Notice that we can rewrite the pumped current as a sum of two terms $I_{p,R}(\theta_1,\theta_2)/I_0 = I^{(0)}(0,0) + I^{(\theta)}(\theta_1,\theta_2)$ consisting of an Aharonov-Bohm flux-dependent part $I^{(\theta)}(\theta_1,\theta_2)$, and a flux–independent part $I^{(0)}(0,0)$. The latter is given by $I^{(0)}(0,0) = rt$ which reaches its maximum value of $I^{(0)}(0,0) = 1/2$ at $t = 1/\sqrt{2}$. The flux-dependent part is a sum of two terms. The second term on the right-hand side of Eq. (8) is proportional to rt and only depends on θ_2. This is a consequence of the chiral nature of transport: If we reverse the direction of transport, this term will only depend on the phase θ_1. From Eq. (8) we also see that the QPC plays an essential role in generating a pumped current. For a closed QPC ($t = 0$) no net pumped current is generated.

For carriers in the low-energy regime, $E \ll \hbar/\delta\tau_i$, we can approximate $\theta_i = (n_{\nu_i} + 1)\pi$. For a transparent point contact, $t = 1$, the pumped current then reduces to $I_{p,R}(\theta_1,\theta_2) = 0$ for $\delta n_- = n_{\nu_1} - n_{\nu_2}$ integer and it achieves maximum values $I_{p,R}(\theta_1,\theta_2)/I_0 = \pm 1$ for δn_- half integer. In the latter, the pump produces a unit I_0 of pumped current which is also its maximum value (for $t = 1$). This is also true for $t = 1/\sqrt{2}$ at $\theta_1 = -\pi/2$ and $\theta_2 = 0$ (modulo 2π). The pumped current reaches a global maximum value of $I_{p,R}/I_0 = \pm(1 + \sqrt{2})/2 \approx 1.2$ at $t = \sqrt{2+\sqrt{2}}/2$.

Figure 2 shows the pumped current as a function of the phase shifts accumulated while traveling around the first and the second superconducting islands for a fixed value of the transparency t of the QPC. The pumped current $I_{p,R}$ clearly is a 2π-periodic function with respect to θ_1 and θ_2. However, as expected from Eq. (8), the pumped current is not a symmetric function under exchange $\theta_1 \leftrightarrow \theta_2$. The pumped current oscillates between positive and negatives values, meaning that the interferometer transmits alternatively electrons and holes. As discussed above, in the low-energy regime the pumped current has values near zero when the phase difference $\delta\theta_- \equiv \theta_1 - \theta_2$ is an even or an odd multiple of π; see lines (a) and (b) in Fig. 2. The asymmetry between the two phases can be seen from the difference between lines

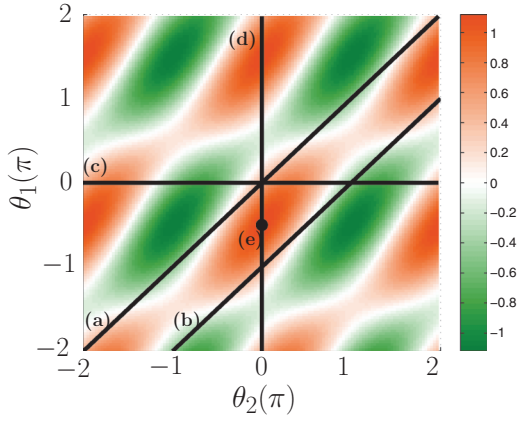

FIG. 2. (Color online) Contour plot of the pumped current $I_{p,R}/I_0$ [Eq. (8)] as a function of the phases θ_1 and θ_2 for $t = 0.8$. (a) $\theta_2 = \theta_1$ line, (b) $\theta_2 = \theta_1 - \pi$ line, (c) $\theta_1 = 0$ line, (d) $\theta_2 = 0$ line, and (e) $\theta_1 = -\pi/2$ and $\theta_2 = 0$ point. The maximum (minimum) values $I_{p,R}/I_0 = \pm 1.12$.

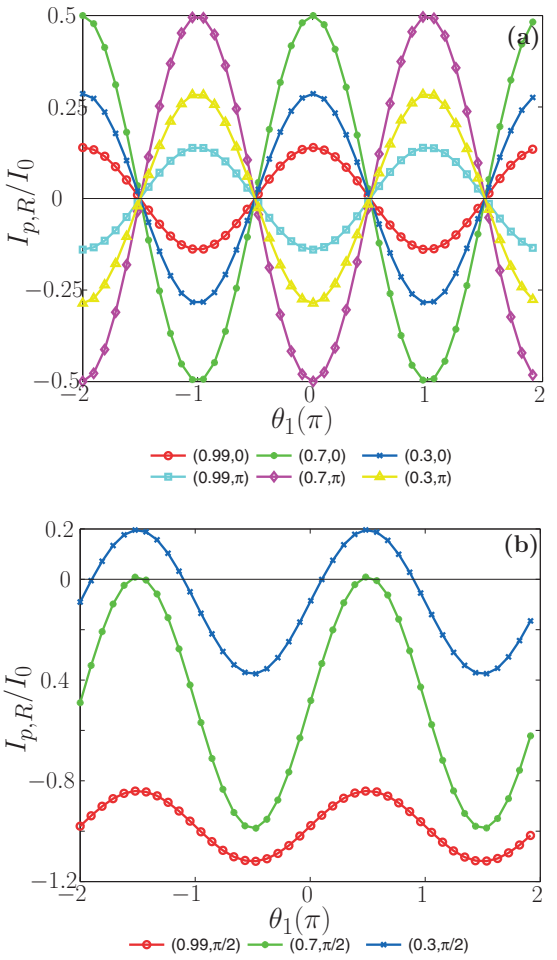

FIG. 3. (Color online) Pumped current [Eq. (8)] as a function of θ_1 for different values of t and for three values of $\delta\theta_- \equiv \theta_1 - \theta_2$. The legend shows the $(t,\delta\theta_-)$ values of each curve in each panel. (a) The top panel shows six curves for (0.99,0), (0.7,0), (0.3,0), (0.99,π), (0.7,π), and (0.3,π). (b) The bottom panel shows three curves for (0.99,$\pi/2$), (0.7,$\pi/2$), and (0.3,$\pi/2$).

(c) and (d) in Fig. 2. The pumped current exhibits maximum values at $\theta_1 = -\pi/2$ and $\theta_2 = 0$ (modulo 2π); see dot (e).

Figure 3 shows the pumped current as a function of θ_1 for different values of t and for three values of $\delta\theta_-$. Figure 3(a) shows the pumped current for $\delta\theta_- = 0$ and $\delta\theta_- = \pi$. The pumped current is symmetric around zero and the addition of a π phase reverses its sign. At multiples of $\theta_1 = \pi/2$, the pumped current goes to zero. Figure 3(b) shows the pumped current for $\delta\theta_- = \pi/2$. In this case, the pumped current is no longer a symmetric function around zero and remains nonzero at multiples of $\theta_1 = \pi/2$.

Conductance. In this section we discuss the difference between the conductance and the pumped current in our system. This is of importance for being able to measure the pumped current, as the main bottleneck for its detection is the difficulty to distinguish between the two types of currents. Using the Landauer-Büttiker formalism[41] the conductance across the interferometer can be written as

$$G(eV) = \frac{e^2}{h}\left(|S^{ee}_{\mathrm{RL}}|^2 - |S^{he}_{\mathrm{RL}}|^2\right). \qquad (9)$$

Using the scattering matrix Eq. (5), the conductance is then given by

$$G(eV) = \frac{e^2}{h}\left(1 - 2\left[t^2 \sin^2\left(\frac{\delta\theta_-}{2}\right) + r^2 \sin^2\left(\frac{\delta\theta_+}{2}\right)\right]\right), \tag{10}$$

where $\delta\theta_\pm \equiv \theta_1 \pm \theta_2$. In the low-energy regime, $E \ll \hbar/\delta\tau_i$, the conductance reaches the limiting values:

$G(0)$	$t = 0\,(\delta n_+)$	$t = 1\,(\delta n_-)$
$\delta n_\pm$ even	$+e^2/h$	$+e^2/h$
$\delta n_\pm$ odd	$-e^2/h$	$-e^2/h$

where $\delta n_\pm \equiv n_{\nu_1} \pm n_{\nu_2}$. When $\delta n_\pm$ is an even number the Majorana states traveling along the two paths are unperturbed and the right normal lead collects an electron. When $\delta n_\pm$ is an odd number, one of the Majorana modes has acquired an additional phase of π and the right lead collects a hole due to crossed Andreev reflection in which a $2e$ charge is absorbed by the superconductors. In both situations, the conductance is sensitive to the number of vortices encircled in the interferometer. This is in agreement with the single Mach-Zehnder interferometer studied earlier.[31,32]

As for the pumped current, the conductance has two contributions: an Aharonov-Bohm flux-independent part and a flux-dependent part, $G(eV) = G^{(0)}(0,0) + G^{(\theta)}(\theta_1,\theta_2)$. The flux-independent term is $G^{(0)}(0,0) = e^2/h$, in which the incident electron is transmitted as an electron. The flux-dependent term has two terms which depend, resp., on the sum and difference of the phases, $\delta\theta_+$ and $\delta\theta_-$. If we reverse the direction of transport, the conductance has the same dependence on θ_i for transport from left to right and from right to left. Thus, the conductance reveals no signature of the chiral nature of transport.

Figure 4 shows the conductance in units of e^2/h as a function of the phase accumulated in the first and second superconducting islands for a fixed value of the transparency of the point contact. Like the pumped current, the conductance is a 2π-periodic function with respect to θ_1 and θ_2. An interesting situation to analyze is when the interferometer does not transmit any charge; i.e., $G(eV) = 0$. This happens in two different situations: first, when the point contact is completely transparent (reflective), $t = 1(0)$, and $\delta\theta_\pm$ is a half integer of π; and second, when $t = r = 1/\sqrt{2}$, $\theta_1 = -\pi/2$, and $\theta_2 = 0$ (modulo 2π). In both cases, the processes of transmitting an electron and transmitting a hole have the same probability to occur. Since these two processes have opposite charge contributions, on average the total charge collected in the right lead is zero. Interestingly, in the second case, at these same points in parameter space the pump generates a maximum current, as discussed earlier.

Figure 5 shows the conductance as a function of θ_1 for different values of t and for three values of $\delta\theta_-$. Figure 5(a) shows the conductance for $\delta\theta_- = 0$ and $\delta\theta_- = \pi$. The conductance remains symmetric around zero and the addition of a π phase changes its sign. Figure 5(b) shows the conductance for $\delta\theta_- = \pi/2$. We see that, in contrast to the pumped current [Fig. 3(b)], the conductance remains a symmetric function

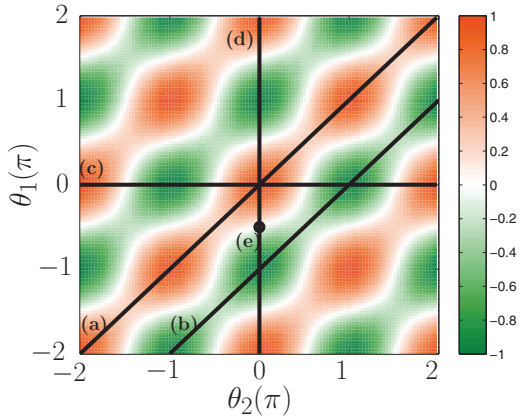

FIG. 4. (Color online) Contour plot of the conductance G [Eq. (10)] in units of e^2/h as a function of the phases θ_1 and θ_2 for $t = 0.8$. (a) $\theta_2 = \theta_1$ line, (b) $\theta_2 = \theta_1 - \pi$ line, (c) $\theta_1 = 0$ line, (d) $\theta_2 = 0$ line, and (e) $\theta_1 = -\pi/2$ and $\theta_2 = 0$ point.

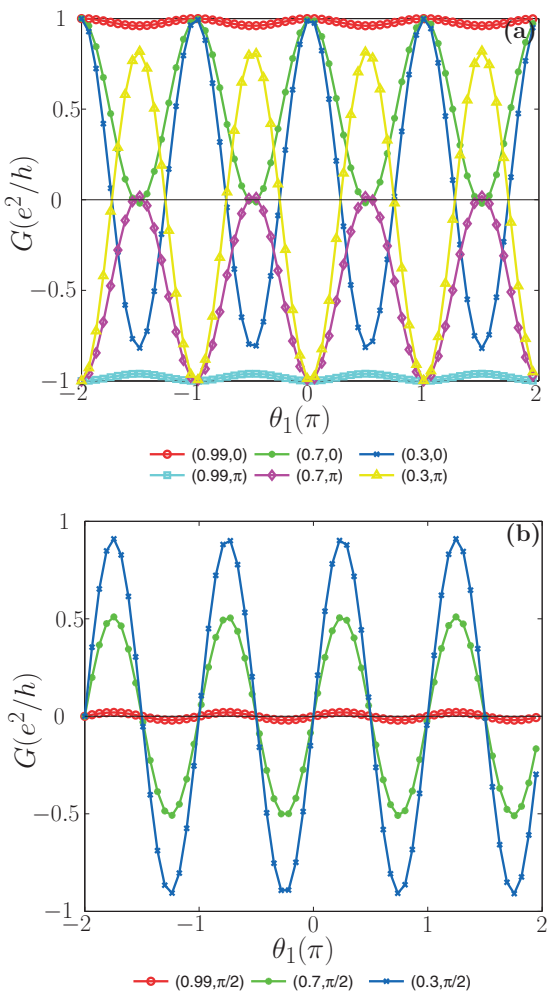

FIG. 5. (Color online) Conductance [Eq. (10)] as a function of θ_1 for different values of t and for three values of $\delta\theta_- = \theta_1 - \theta_2$. The legend shows the $(t,\delta\theta_-)$ values of each curve in each panel. (a) The top panel shows six curves for (0.99,0), (0.7,0), (0.3,0), (0.99,π), (0.7,π), and (0.3,π). (b) The bottom panel shows three curves for (0.99,$\pi/2$), (0.7,$\pi/2$), and (0.3,$\pi/2$).

around zero and that for any value of t, the conductance becomes zero at multiples of $\theta_1 = \pi/2$.

We thus predict three main differences between the conductance and the pumped current in this system: (1) Although the conductance and the pumped current both contain a flux-independent part and a flux-dependent part, the flux-independent part of the conductance is independent of any system parameters while the flux-independent part of the pumped current depends on the transparency of the point contact. (2) While the conductance is insensitive to the direction of transport, the magnitude of the pumped current depends on whether the current is collected in the right or left lead, thereby reflecting the chiral nature of the transport. (3) At certain points in parameter space (i.e., for certain values of t, θ_1, and θ_2), the conductance is zero, whereas the pumped current reaches maximum values.

The proposed pumping mechanism requires the phases θ_1 and θ_2 to be varied in a periodic manner. One way to achieve this would be by periodically varying the magnetic field in each superconducting island. Alternatively, the velocity of the chiral Majorana states could be changed, using the method proposed in Ref. 14.

Conclusions. To summarize, we have analyzed quantum pumping via Majorana fermions in a Mach-Zehnder interferometer formed by ferromagnetic and superconducting regions on top of a 3D topological insulator. We have shown that in the low-energy regime the pumped current, unlike the conductance, cannot be used to distinguish between an even or odd number of Majorana bound states at the vortex cores in the superconducting islands. The pumped current, however, can be used to reveal signatures of the chiral nature of transport, whereas the conductance is independent of the direction of transport. We have also shown that the pumped current reaches maximum values in certain regions of parameter space where the conductance becomes zero. Tuning the system into the latter regions thus creates chances for experimentally observing the adiabatically pumped current induced by Majorana modes in this system.

Acknowledgments. We would like to thank A. Saha and C. Bruder for valuable discussions. This research was supported by the Dutch Science Foundation NWO/FOM. R.P.T. acknowledges financial support by the Swiss SNF and the NCCR Quantum Science and Technology.

[1] J. Alicea, Rep. Prog. Phys. **75**, 076501 (2012).
[2] M. Leijnse and K. Flensberg, Semicond. Sci. Technol. **27**, 124003 (2012).
[3] C. Beenakker, Annu. Rev. Condens. Matter Phys. **4**, 113 (2013).
[4] T. D. Stanescu and S. Tewari, J. Phys.: Condens. Matter **25**, 233201 (2013).
[5] G. Moore and N. Read, Nucl. Phys. **360**, 362 (1991).
[6] A. Stern, Nature (London) **464**, 187 (2010).
[7] D. A. Ivanov, Phys. Rev. Lett. **86**, 268 (2001).
[8] J. D. Sau, R. M. Lutchyn, S. Tewari, and S. Das Sarma, Phys. Rev. Lett. **104**, 040502 (2010).
[9] J. D. Sau, S. Tewari, R. M. Lutchyn, T. D. Stanescu, and S. Das Sarma, Phys. Rev. B **82**, 214509 (2010).
[10] J. Alicea, Phys. Rev. B **81**, 125318 (2010).
[11] M. Z. Hasan and C. L. Kane, Rev. Mod. Phys. **82**, 3045 (2010).
[12] X.-L. Qi and S.-C. Zhang, Rev. Mod. Phys. **83**, 1057 (2011).
[13] L. Fu and C. L. Kane, Phys. Rev. Lett. **100**, 096407 (2008).
[14] R. P. Tiwari, U. Zülicke, and C. Bruder, Phys. Rev. Lett. **110**, 186805 (2013).
[15] B. Sacépé, J. B. Oostinga, J. Li, A. Ubaldini, N. J. Couto, E. Giannini, and A. F. Morpurgo, Nat. Commun. **2**, 575 (2011).
[16] M. Veldhorst, M. Snelder, M. Hoek, T. Gang, V. K. Guduru, X. L. Wang, U. Zeitler, W. G. van der Wiel, A. A. Golubov, H. Hilgenkamp *et al*., Nat. Mater. **11**, 417 (2012).
[17] F. Qu, F. Yang, J. Shen, Y. Ding, J. Chen, Z. Ji, G. Liu, J. Fan, X. Jing, C. Yang, and L. Lu, Sci. Rep. **2**, 339 (2012).
[18] J. B. Oostinga, L. Maier, P. Schüffelgen, D. Knott, C. Ames, C. Brüne, G. Tkachov, H. Buhmann, and L. W. Molenkamp, Phys. Rev. X **3**, 021007 (2013).
[19] E. J. H. Lee, X. Jiang, M. Houzet, R. Aguado, C. M. Lieber, and S. D. Franceschi, Nature Nanotechnology **9**, 79 (2014).
[20] K. Sengupta, I. Žutić, H.-J. Kwon, V. M. Yakovenko, and S. Das Sarma, Phys. Rev. B **63**, 144531 (2001).
[21] C. J. Bolech and E. Demler, Phys. Rev. Lett. **98**, 237002 (2007).
[22] K. T. Law, P. A. Lee, and T. K. Ng, Phys. Rev. Lett. **103**, 237001 (2009).
[23] K. Flensberg, Phys. Rev. B **82**, 180516 (2010).
[24] V. Mourik, K. Zuo, S. M. Frolov, S. R. Plissard, E. P. A. M. Bakkers, and L. P. Kouwenhoven, Science **336**, 1003 (2012).
[25] A. Das, Y. Ronen, Y. Most, Y. Oreg, M. Heiblum, and H. Shtrikman, Nat. Phys. **8**, 887 (2012).
[26] M. T. Deng, C. L. Yu, G. Y. Huang, M. Larsson, P. Caroff, and H. Q. Xu, Nano Lett. **12**, 6414 (2012).
[27] H. O. H. Churchill, V. Fatemi, K. Grove-Rasmussen, M. T. Deng, P. Caroff, H. Q. Xu, and C. M. Marcus, Phys. Rev. B **87**, 241401 (2013).
[28] A. D. K. Finck, D. J. Van Harlingen, P. K. Mohseni, K. Jung, and X. Li, Phys. Rev. Lett. **110**, 126406 (2013).
[29] L. P. Rokhinson, X. Liu, and J. K. Furdyna, Nat. Phys. **8**, 795 (2012).
[30] J. R. Williams, A. J. Bestwick, P. Gallagher, S. S. Hong, Y. Cui, A. S. Bleich, J. G. Analytis, I. R. Fisher, and D. Goldhaber-Gordon, Phys. Rev. Lett. **109**, 056803 (2012).
[31] L. Fu and C. L. Kane, Phys. Rev. Lett. **102**, 216403 (2009).
[32] A. R. Akhmerov, J. Nilsson, and C. W. J. Beenakker, Phys. Rev. Lett. **102**, 216404 (2009).
[33] G. Strübi, W. Belzig, M.-S. Choi, and C. Bruder, Phys. Rev. Lett. **107**, 136403 (2011).
[34] M. Büttiker, H. Thomas, and A. Prêtre, Z. Phys. B **94**, 133 (1994).
[35] P. W. Brouwer, Phys. Rev. B **58**, R10135 (1998).
[36] B. Spivak, F. Zhou, and M. T. Beal Monod, Phys. Rev. B **51**, 13226 (1995).
[37] M. Gibertini, R. Fazio, M. Polini, and F. Taddei, Phys. Rev. B **88**, 140508 (2013).
[38] M. Blaauboer, Phys. Rev. B **65**, 235318 (2002).
[39] J. Wang and B. Wang, Phys. Rev. B **65**, 153311 (2002).
[40] J. Li, G. Fleury, and M. Büttiker, Phys. Rev. B **85**, 125440 (2012).
[41] Y. V. Nazarov and Y. M. Blanter, *Quantum Transport: Introduction to Nanoscience* (Cambridge University Press, Cambridge, 2009).